Diameter-dependent wetting of tungsten disulfide nanotubes

Ohad Goldbart[a], Sidney R. Cohen[b], Ifat Kaplan-Ashiri[b], Polina Glazyrina[c], H. Daniel Wagner[a], Andrey Enyashin[c,d,1], and Reshef Tenne[a,1]

[a]Department of Materials and Interfaces, Weizmann Institute of Science, Rehovot 76100, Israel; [b]Department of Chemical Research Support, Weizmann Institute of Science, Rehovot 76100, Israel; [c]Institute of Mathematics and Computer Sciences, Ural Federal University, Ekaterinburg 620083, Russia; and [d]Institute of Solid State Chemistry, Ural Branch of the Russian Academy of Sciences, Ekaterinburg 620990, Russia

Edited by Charles M. Lieber, Harvard University, Cambridge, MA, and approved October 17, 2016 (received for review May 5, 2016)

The simple process of a liquid wetting a solid surface is controlled by a plethora of factors—surface texture, liquid droplet size and shape, energetics of both liquid and solid surfaces, as well as their interface. Studying these events at the nanoscale provides insights into the molecular basis of wetting. Nanotube wetting studies are particularly challenging due to their unique shape and small size. Nonetheless, the success of nanotubes, particularly inorganic ones, as fillers in composite materials makes it essential to understand how common liquids wet them. Here, we present a comprehensive wetting study of individual tungsten disulfide nanotubes by water. We reveal the nature of interaction at the inert outer wall and show that remarkably high wetting forces are attained on small, open-ended nanotubes due to capillary aspiration into the hollow core. This study provides a theoretical and experimental paradigm for this intricate problem.

wetting | inorganic nanotubes | capillary | MD simulations | in situ microscopy

Wetting of solid surfaces is an intricate and subtle phenomenon that is fundamental to many fields ranging from lubrication to composite materials to capillary effects (1, 2). In recent years, unique nanoscale aspects of wetting have been revealed, highlighting the importance of a molecular-level understanding of wetting. Theoretical studies based on molecular dynamics (MD) and Monte Carlo simulations revealed that the macroscale theory of wetting may deviate from the nanoscale behavior for particular surface geometries and droplet sizes (3). A comprehensive review distinguished two size-related effects. Continuum hydrodynamics of simple liquids is valid down to the nanometer length scale, whereas surface effects can influence at larger scales (4). In addition, experiments have detected heterogeneity in the nanowetting properties of ostensibly similar individual nanoparticles. This behavior was attributed to nanoscale surface properties such as chemistry, shape, and topography (5).

Study of nanotube wetting is an exciting endeavor, the first step in their incorporation as fillers into ultrastrength nanocomposites. Wetting interactions of nanotubes with different liquids (6–8), polymers (9), and many other materials have been examined both theoretically and experimentally (10–13). Chemical interactions, geometrical and structural factors come into play in such studies (14). For instance, enhanced wetting of carbon nanotubes (CNTs) (15) with open end has been attributed to capillary suction of water into the hollow stem of the nanotube (16). Inorganic WS_2 and MoS_2 nanotubes (INTs) (17) were shown to disperse very well in a variety of polymers, enabling preparation of nanocomposites with enhanced mechanical properties (18), thermal stability (19), and improved rheological behavior (20). Nonetheless, the nature of the interaction between an individual nanotube and polymer liquid has received little attention and is poorly understood, partly due to the technological challenge posed by such studies.

Here, we report a combined experimental and theoretical study on the microscopic interaction of WS_2 nanotubes (INT-WS_2) with water. We apply a unique experimental approach based on manipulation and pullout of individual nanotubes from water films using both environmental scanning electron microscopy (ESEM) and atomic force microscopy (AFM) techniques. Detailed theoretical calculations based on density functional theory (DFT) and force-field MD simulations together with thermodynamic analysis provide strong support for water capillary effect. Furthermore, MD simulations show that the general behavior seen for water occurs also for carbon tetrachloride. The overall interaction energy exhibited a clear trend with nanotube diameter, due to capillarity within the open-ended tubes and influence of their curvature.

Results and Discussion

Two kinds of INT-WS_2 were investigated: type I nanotubes were <40 nm in diameter and 1–3 μm long, consisted of up to 10 walls, and had a hollow core with an open end. Type II nanotubes were 40–150 nm in diameter, 2–30 μm long, with up to 30 walls. The latter were generally capped and partially filled with an oxide at the core. Typical micrographs of each type are shown in Fig. 1 *A* and *B*.

The interaction of water with bulk and single-layer (graphene-like) WS_2 and MoS_2 surfaces has been recently studied (21–23). To learn about the interaction of the WS_2 nanotubes with water, the contact angle (θ) of water on the (outer) surface of individual INT-WS_2 was directly measured inside an ESEM by condensing water on the nanotubes at ~4 °C (Fig. 1*C*).

The small water droplets that condensed on the cooled nanotubes were subsequently measured—for ~30 such droplets, the average measured contact angle was $\theta = 60° \pm 8°$, compared

Significance

The wetting of solid surfaces by liquids is of great interest in scientific fields ranging from lubrication to the strength of composite materials. These interactions can change dramatically at the nanoscale, impacting on current development of novel devices and materials. We have studied the wetting of individual, size-selected tungsten disulfide nanotubes, both experimentally and theoretically. The results show that wetting forces and free energy can vary by orders of magnitude when capillary action is enhanced in open-ended vs. closed-ended nanotubes, as deduced from the influence of specific nanotube size and geometry in governing the final wetting properties. This work provides a comprehensive view of the molecular-level interactions involved in nanotube wetting.

Author contributions: O.G., S.R.C., I.K.-A., P.G., and A.E. designed research; O.G., S.R.C., P.G., and A.E. performed research; I.K.-A. and R.T. contributed new reagents/analytic tools; O.G., S.R.C., P.G., A.E., and R.T. analyzed data; and O.G., S.R.C., H.D.W., A.E., and R.T. wrote the paper.

The authors declare no conflict of interest.

This article is a PNAS Direct Submission.

[1]To whom correspondence may be addressed. Email: reshef.tenne@weizmann.ac.il or enyashin@ihim.uran.ru.

This article contains supporting information online at www.pnas.org/lookup/suppl/doi:10.1073/pnas.1607202113/-/DCSupplemental.

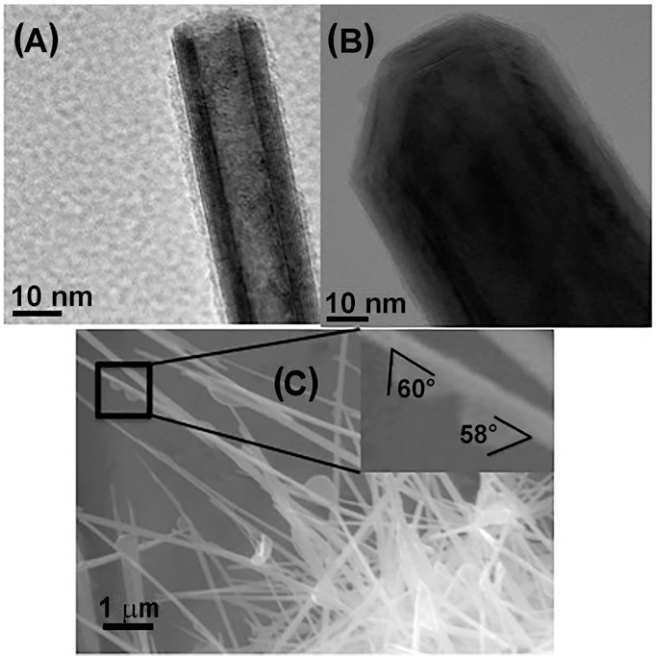

Fig. 1. TEM micrograph of the two kinds of WS_2 nanotubes used in this series of experiments. (*A*) A 30-nm-diameter INT with open cap and no oxide filling (type I); (*B*) A 100-nm INT, with large number of outer walls and a closed cap (type II). (*C*) SEM image of condensed water droplets on an assortment of cooled (type II) WS_2 nanotubes. In the *Inset*, zoom-in on two single water droplets and their manually measured contact angles.

with a contact angle of 70° found for a clean flat layer of WS_2 (21). Because water is known to bind well to dangling bonds on metal dichalcogenides, this result attests to the defect-free nature of the nanotube walls. Comparable results were obtained for a monolayer of MoS_2, showing that water does not adsorb on the defect-free surfaces of MoS_2 (21, 23). Thus, the interaction between water and the defect-free nanotube wall is weak. To investigate the difference in water–tubule interactions between the nanotube wall and its end, as well as to probe the microscopic mechanism of the solid–liquid interaction, we next measured the pullout forces of individual nanotubes dipped into a fluid bath. For this purpose, the nanotubes were attached to a force-transducer (AFM cantilever) as described in *Materials and Methods* and *S2. WS_2 Nanotube Pullout Measurements*.

ESEM Experiments. A single WS_2 nanotube attached to a cantilever tip was manipulated until it reached the proximity of a water film that was condensed on a cooled stainless-steel stub (further details of the experimental setup in *S2. WS_2 Nanotube Pullout Measurements*; schematic rendering of the setup in Fig. S1). Then the tip was gently manipulated toward the water film until the INT made contact with the film, allowing the film to spontaneously wet the nanotube (Fig. 2*A* and Figs. S2 and S3). At this point, the nanotube was pulled backward using the nanomanipulator in steps of ∼10 nm every 5–10 s. While pulling out the INT (type I), a surprisingly large water meniscus, with a cone-like shape, was obtained (Fig. 2*B* and Movie S1). Such movies reveal that the interaction is with the tip of the nanotube, and there is no visible accumulation of water along the nanotube walls. The INT was pulled continuously outward until it snapped out and separated from the water film (Fig. 2*C*). The maximum height of the water meniscus was denoted as l (Fig. 2*B*), and the total distance traversed by the INT tip (from initial to the final point) is X (Fig. 2*C*). The force required to pull out the nanotube was calculated according to Hooke's law and expressed as $F_{max} = (X - l)^* k$, where k is the calibrated spring constant of the cantilever. The work is calculated by integrating the force with distance traveled until separation of water meniscus. This calculation makes the assumption that the water surface "grabs" the NT at a fixed point on its surface and there is no slip during pullout. The assumption is reasonable considering the discussion surrounding the MD simulations below showing that the main attraction of water is at tube apex.

The experimental work done by the cantilever during the pullout, computed as described in *Materials and Methods*, can be compared with the calculated work of formation of the water meniscus, the surface area of which is mathematically approximated as a catenoid of revolution (*S3. Phenomenological Estimation of the Surface Energy of the Water Meniscus Beneath the Pulled-Out Nanotube Tip*). Two parameters were determined in the experiment, namely, the height of the water "cone," l, and the radius of its base, $D_c/2$ (Fig. S4). Using Eq. **S4**, these two parameters were used to calculate the surface area of the water "cone." Multiplying this area by the surface tension of water, $\gamma = 72.3$ mJ/m^2, gives the work expended in forming the meniscus. The results are summarized in Table 1. Good correspondence between the measured and calculated quantities was obtained.

AFM Experiments. Similar single nanotube pullout experiments were also carried out using an AFM setup (*S2. WS_2 Nanotube Pullout Measurements*, *S2.2. AFM Pullout Measurements*). The AFM experiments allow on-line monitoring of the wetting force and can be done under ambient (equilibrium) conditions. In the present experiment, a nanotube was attached to an AFM tip and lowered toward a water reservoir. The AFM was programmed to lower the nanotube tip until sensing a "jump-in" (the initial contact point). This small deflection represents (for the larger diameters, see below) the wetting force of the nanotube wall. This force should correspond to that predicted by the Wilhelmy balance technique (6). Indeed, presuming a wetting angle of 60° for the 90-nm-diameter nanotube, we predict initial wetting force of 20 nN compared with 23 nN actually measured. At this point, the nanotube was pulled back out of the water by retraction of the z-piezo, while recording the AFM cantilever deflection.

According to the Wilhelmy balance formulation, the wetting force on the nanotube should not change throughout the pullout as long as the contact perimeter remains constant. Because the ultimate pullout force is dominated by the meniscus growth that occurs as the water surface is pinned to the nanotube end, we must consider here specifically the geometry of the nanotube tip. To compare the pullout forces, they were normalized by the nanotube cross-sectional area at its end. As shown earlier, the walls of the INT do not seem to interact strongly with water, but the tip apex does. Therefore, the relevant normalization area is calculated as $\pi/4(D_{out}{}^2 - D_{in}{}^2)$, where D_{out} and D_{in} are the outer and inner diameters of the nanotube, respectively. Note that, for type II nanotubes, $D_{in} = 0$. A detailed explanation appears in *S2. WS_2 Nanotube Pullout Measurements*, *S2.1. ESEM Pullout Measurements*. The normalized force was plotted against the nanotube diameter, and the results are presented in Fig. 3*A*, incorporating the results from both the AFM and ESEM setups. Pullout work

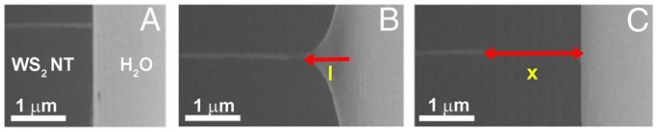

Fig. 2. (*A*) Initially, the INT-tip touches the surface of the water film. (*B*) Just before the snapping out of the nanotube-tip from the water "cone" (denoted as the maximum force point, *l*). (*C*) Image of the water film and the nanotube right after the separation; the position of the edge of the tube represents the overall distance traveled by the cantilever during pullout (*X*).

Table 1. Comparison of experimental and calculated pullout work

Nanotube diameter, nm	Calculated work, fJ	Cantilever work, fJ
70	50	23 (7)
90	69	47 (14)
100	81	66 (20)

Experimental nanotube diameters were within 1 nm of the values reported here. The calculated work was computed from the calculated area of catenoid of revolution and surface tension of water, based on the ESEM image of meniscus. For the cantilever work the experimental uncertainty is presented in parentheses.

was computed for the AFM measurements as with ESEM results, with the exception that here the ultimate force was measured in real time by recording the cantilever deflection and the force during pullout was modeled as decaying linearly with distance.

Although the ESEM and AFM experiments exhibit the same trend for the normalized pullout forces, the pullout forces are significantly lower for the ESEM experiments for the two smallest diameter nanotubes. This difference can be possibly attributed to the different ambient conditions in the ESEM and AFM pullout experiments: the very small radius of the liquid contact leads to enhanced vapor pressure of the water meniscus, which is described by the Kelvin equation (24). Due to the partial vacuum in the ESEM, we can expect even more rapid evaporation and earlier collapse of the water meniscus. As a result, the contact area of this small volume decreases rapidly during the ESEM measurements and the water neck breaks at a lower cantilever force, compared with the ambient AFM experiments. In any event, the graph shows a clear distinction between the type I and type II nanotubes. Wetting forces of the former show almost no dependence on size, albeit some variations for the three largest diameter nanotubes are observed, which can be attributed to defects at the NT cap that resulted in a collapse and possible small crack. This is discussed in *S4. Collapse of Large-Diameter Nanotubes*, and shown in Fig. S5. Such fluctuations in force, as well as in work (see next section and Fig. 3*B*), are small relative to the differences seen for small-diameter nanotubes. For the type I nanotubes, there is a dramatic rise in force with lower diameter. These forces, normalized to the cross-sectional area, are on the order of 1–2 GPa, which approaches the strength of the nanotubes, ~6–20 GPa (25). Indeed, in some cases, we observed breakage of the nanotube after the water pullout. These results lead to a hypothesis of strong capillary forces inside the small, open nanotubes. To investigate this microscopic phenomenon, we made use of atomistic calculations.

DFT Calculations. To better understand the results of these pullout experiments, DFT calculations were undertaken. First, the interaction energies between water surface and the edge of a WS_2 slab with dangling bonds were calculated. Subsequently, the interaction energies for INTs of different diameters were calculated by extrapolation from the previous detailed calculations and are shown in Fig. 3*B*. Details of the calculations are provided in *S5. DFT Calculations*, and in Figs. S5–S10. These energies are compared with the work of formation of the meniscus. Formally, a force balance should be performed to equate the force applied by the cantilever with the force required to break the water bridge. Due to changing volume of the liquid throughout the pullout, this cannot be quantified simply in terms of forces. We therefore compare energies rather than forces with the implicit assumption that the energy released by relaxation of the meniscus compensates the energy lost by breaking the nanotube–water interaction. The results show good agreement with type II nanotubes over a wide range of diameters but were almost insensitive to diameter of the nanotubes. There is, however, a large discrepancy for type I INTs and a minor difference for the type II INTs with the largest diameters. For example, the calculation for a WS_2 nanotube with diameter of 25 nm and composed of 10 walls yields a total binding energy around 0.52 fJ (Fig. S7). This value is ~10^3 times smaller than 195 fJ calculated for the surface energy (i.e., work of formation) of the rising water meniscus in the experiment.

It can be therefore concluded from the DFT calculations that the interaction of the nanotube tip outer wall is not sufficiently strong to account for the strong binding with the water, in particular for the small-diameter, open-ended (type I) nanotubes. Even the presence of reactive W atoms at the tip, as considered in these models, cannot alone lead to a binding energy commensurate with the surface energy of the water meniscus that develops during pullout.

MD Simulations. To investigate the hypothesis of capillary suction of water into the hollow core of the open-ended nanotubes, detailed MD simulations were carried out. The MD simulations of the water–WS_2 nanotube interactions were performed in two main modes. In mode 1 simulation, imbibition of an isolated water drop into an open-ended (24,0)@(36,0) 2H–WS_2 double-wall nanotube tip with inner and outer diameters of 24.2 and 36.2 Å (measured for the W atomic cylinders), was studied. Both the case of S-terminated inner and W-terminated outer wall (I) and the opposite situation were considered (II) (Fig. S8). The MD simulations showed, for case (I), instantaneous (weak) water adsorption with H atoms pointing to the tip. For case (II), the exposed inner W atoms were decorated by H_2O molecules with the O atom of the water between two W atoms and the formation of a labile circular water chain (the average W–O distance in this case is about 2.5 Å) along the tip circumference. Labile

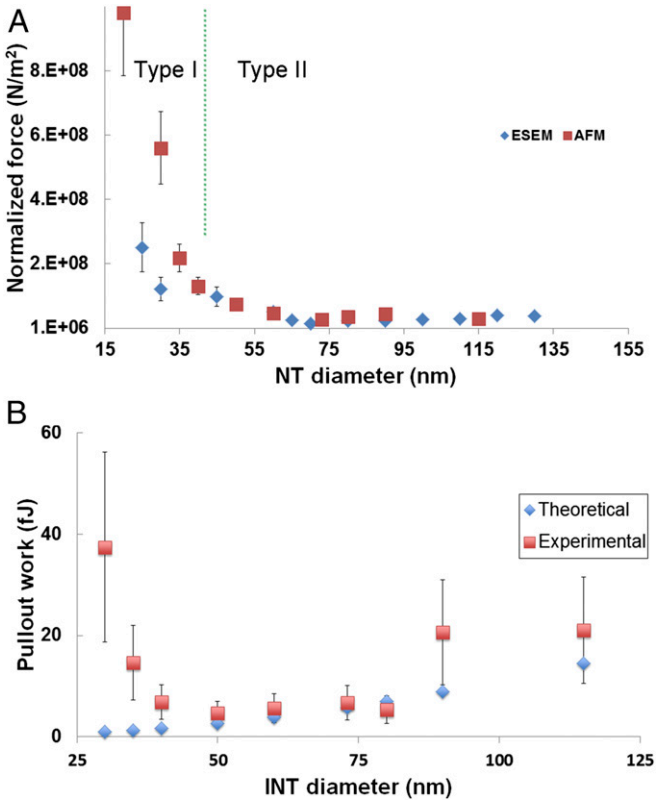

Fig. 3. (*A*) Normalized pullout forces of INT measured in ESEM (blue rhombi) and AFM (red squares). (*B*) Pullout work vs. the nanotube (outer) diameters. Blue rhombi are the results calculated by the DFT calculations. Red squares are results calculated from the AFM pullout experiments (see text).

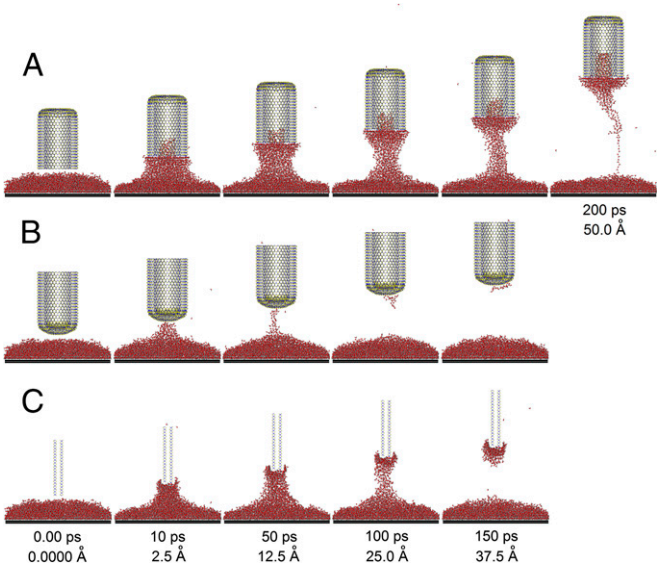

Fig. 4. Side-view screenshots of the MD simulations of pullout tests from the surface of water film using WS_2 nanotips of different morphology: open-ended (24,0)@(36,0) nanotube (*A*), capped (24,0)@(36,0) nanotube (*B*), and double-walled (32,0) nanostripe (*C*). The MD time and the distance of the tip withdrawn from the film are shown below.

chain-like water fragments could be observed on the outer surface of nanotubes, although they mostly remained confined to the tube apex region and did not coalesce into a stable outer coating on the basal sulfur surface of the nanotube (Fig. S8). In general, fast kinetics of water imbibition into the hollow core of the WS_2 nanotube, following the $(t)^{1/2}$ rule (26), was observed for both cases (water imbibition in case I was 1.5 times faster compared with case II; see further details in *S6. MD Simulations*). The analysis of the radial distribution functions for O and H atoms within a nanotube shows that the water remains as a liquid and did not crystallize in the confined space of the hollow core. To summarize these simulations, MD has convincingly shown rapid capillary penetration of water into the hollow stem of narrow and open-ended (type I) WS_2 nanotubes irrespective of the exposed atom at the edge of the tube. Therefore, the capillary kinetics is irrelevant to the steady-state pullout situation studied here.

In mode 2, the retraction of a nanotube tip from the water film has been considered, for different model structures. The starting models in the present study were again double-walled (24,0)@(36,0) nanotubes with 2H–WS_2 polytypic arrangement (Fig. S9). To emphasize the edge effect of the nanotubes with respect to capillarity, three cases were considered—open-ended and capped nanotubes and a nanostripe of similar size. Due to inadequate computer resources, the MD simulations were limited to small systems compared with experiment and have been launched with the nanotube tip and water film already in contact. These MD calculations capture the salient features of the water–nanotube interaction during pullout, shedding insight on the interaction between the water surface and a pulled-out nanotube (Fig. 4).

The direct visualization of the tip pullout reveals the multistage character of this process (Fig. S10 and Movie S2). First, water molecules did not climb up the outer surface of the receding nanotube in any of the cases studied here. On the other hand, the strong capillary interaction between the open-ended INT tip and the water is clearly visible in Fig. 4*A*. Significantly, the water continues the ascent during the entire pullout process, even after the nanotube has disengaged from the water surface. The water catenoid formed near the open-ended nanotube tip exhibits mechanical instability (asymmetric shape) at a distance of 25 Å and is fully separated from the tip at a distance of 50 Å.

When using capped nanotubes, quite different behavior is observed (Fig. 4*B* and Movie S3). First, the retraction of the tip is not accompanied by strong attraction of water molecules. Only a small meniscus is formed during the pullout, which is attributed to the weak water cap interaction. The instability of the small meniscus occurs around 12 Å, in this case. The water meniscus narrows very quickly upon pullout and disappears at a small separation of the tip from the water surface. It is important to note that the present model of the capped nanotubes does not take into account the imperfections in the cap and residual WO_x solid that are more common in the core of the very large-diameter nanotubes, both of which would increase the adhesion energy of the tip with water. The pullout of a nanostripe tip shows some similarities to the features of an open-ended WS_2 nanotube (Fig. 4*C*; *S6. MD Simulations, S6.2. Comments on the MD Simulations*; Movie S4) without the capillary action. The water molecules do not ascend along the wall and a complete breakup of the water–tip contact is observed only at 36 Å.

To minimize computer resources, the models were restricted in size, and hence the water meniscus was much smaller than in the experiments. Thus, the absolute values of the forces should be smaller than the measured ones. However, the MD simulation predicts the same tendency for the affinity of the receding WS_2 tips with respect to water with maximum forces of 2.11, 0.34, and 1.76 nN for the open and capped nanotubes and the nanostripe, respectively.

Because water is an atypical liquid, with relatively high surface tension and influence of hydrogen bonding, we have also carried out MD simulations for a nonpolar, centrosymmetric molecule, CCl_4. The same overall features as observed for water occur (meniscus formation upon pullout as well as capillary imbibition into the hollow nanotube core). However, the CCl_4 has a much higher affinity to the outer walls of the nanotube, so that partitioning of energy contributions for the inner and outer liquid bridges is of approximately equal weight. Pullout videos for open and closed nanotubes pulled out from a thin film of carbon tetrachloride are shown in Movies S5 and S6.

Thermodynamic Analysis. The difference in free energy ΔG between n moles of liquid within the cavity and the same n moles of liquid on a flat surface can be expressed as follows:

$$\Delta G = n(\mu(r) - \mu(\infty)) = nRT \cdot \ln\left[\frac{p_r}{p_\infty}\right], \qquad [1]$$

where μ and p are the chemical potentials and vapor pressures for the liquid within a cavity and for the flat surface (indices r and ∞, respectively). Using the Young–Laplace equation (see *S7. Thermodynamics Model*, for full details of the analysis), the capillary work of the water within the nanotube can be expressed as follows:

$$\begin{aligned}\Delta G &= \frac{\pi\rho}{4M_r} RTD_{in}^2 h \cdot \ln\left(1 - \frac{4\gamma}{p_\infty D_{in}}\cos\theta\right) \\ &= 0.107 \cdot (D_{out} - 1.23k)^2 h \cdot \ln\left(1 - \frac{2{,}854.577}{[D_{out} - 1.23k]}\cos\theta\right),\end{aligned} \qquad [2]$$

where, D_{in} and D_{out} are inner and outer diameters, k is the number of WS_2 layers composing the wall of nanotube. h is the height of ascending capillary column; γ, ρ, and M_r are surface tension, density, and molecular weight (at temperature T = 296 K) for water. $\gamma = 72.31 \cdot 10^{-3}$ N/m^2, $\rho = 0.99754 \cdot 10^3$ kg/m^3, and T and p_∞ correspond to temperature and external pressure. Because the argument of the logarithm is limited to positive values, the wetting angle θ must be less than 90°. The use of macroscopic values of γ is justified because the surface tension of water grows significantly only for curvature radii below ~2 nm (27). Second, for

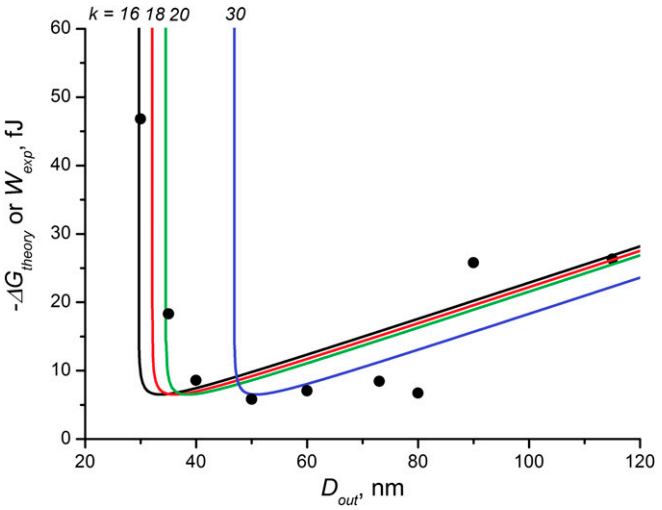

Fig. 5. Plot of the capillary energy ΔG estimated for water imbibition into WS_2 nanotubes with length $h = 250$ nm, vs. inner diameter (determined by the outer diameter of nanotube D and the number of layers comprising the wall, k. The wetting angle between H_2O and the inner core of the WS_2 nanotube is assumed to be 89.80°. Experimental values of the pullout work W obtained after AFM measurements are plotted for comparison as the black dots with the black curve serving only as a guide for the eye.

the diameters of nanotubes used in the present experiments, water penetrates along the full length of the nanotube cavity, h (28), which is taken here to be 250 nm. The work of capillary action of water inside the nanotube is plotted vs. diameter for different numbers of walls in Fig. 5.

A suitable fit of thermodynamic model to the experimental data is possible only if the contact angle is at the hydrophobic/hydrophilic limit, that is, close to 90°, higher than the value 60–70° observed from direct ESEM observations or measured on planar WS_2. This discrepancy reflects the decrease of $\cos\theta$ for high curvature of a liquid surface, here the water meniscus in the WS_2 nanotube. This trend was suggested in earlier theoretical models and recent MD simulations (29, 30).

Because only the small-diameter tubes have open ends, the analysis of capillary action presented in Fig. 5 is mostly relevant for them. The fact that, for the 20-nm diameter nanotube, the experimental pullout work was 500 fJ, and in some cases such small nanotubes were found to be broken after the experiment, suggests that the capillary force exceeded their strength (~6–20 GPa). These results conform well with the extrapolation of the thermodynamic analysis, which provides independent support for the idea that a major contribution for the pullout work of small-diameter (type I) tubes comes from the capillary imbibition of water into the hollow core of the nanotubes.

This work presents a systematic study of the interactions between individual WS_2 nanotubes and water or any other liquid. Two different experimental setups (ESEM and AFM) were used showing the marked difference between slender and open-ended tubes (type I) and large-diameter and capped nanotubes (type II). Different theoretical approaches, namely, DFT, MD, and thermodynamic considerations were used to analyze the experimental data. Semiquantitative agreement was obtained between the DFT analysis and the experimental data for large-diameter (type II) tubes. However, the small-diameter nanotubes with open end (type I) deviated considerably from the interaction energy predicted by DFT. MD analysis, although limited to small-diameter tubes and overall small model size compared with the experiment, showed unequivocally that capillary action between the water and the open-ended nanotubes stimulates penetration of the water molecules into the hollow core and their fast ascent, leading to substantially larger energy for the pullout work. Obviously, the present framework is applicable to various types of nanoparticles and liquids and not constrained to INT and water. Preliminary results presented here using CCl_4 show a similar capillary imbibition and meniscus formation, although the affinity of the CCl_4 for the nanotube wall leads to near-equal energy partition between inner and outer liquid interactions. These results form a comprehensive framework for studying the interaction between single nanoparticle and liquefied matrices that could provide a deeper understanding of nanocomposite behavior. Furthermore, open-ended WS_2 nanotubes can be used as nanopipettes and nanosensors. For example, a single nanotube could aspirate about 10^6 water molecules. By incorporating such a nanotube in a field effect transistor device (31), we estimate that detection of <10 contaminant molecules can be achieved.

Materials and Methods

The WS_2 nanotubes were of two types: type I nanotubes were produced by fluidized-bed reactor, resulting in nanotubes with diameter <40 nm and containing up to 10 walls (32). Type II nanotubes ranged between 40- and 150-nm diameter with up to 30 walls and were produced in a one-pot process (33).

Single Nanotube AFM Tip Fabrication. All of the pullout experiments (ESEM and AFM) were performed using calibrated AFM probes with single INT-WS_2 nanotubes attached to the tip. For the attachment of the nanotube, INT-WS_2 powder was dispersed on the edge of a platinum-coated razor blade (Fig. S1). Using a nanomanipulator, the calibrated AFM tip is manipulated to the edge of the blade where the INTs hang out from the edge. Using the manipulator, the nanotube was adjusted to an angle of ~15° with the cantilever normal to compensate for the angle of the cantilever holder, and ensure vertical immersion of nanotube into the liquid. The edge of the AFM tip is attached to the distal end of a single INT-WS_2 using a 200-nm-thick layer of evaporated platinum, binding the nanotube firmly to the tip (Fig. S1). The platinum "glue" is deposited in a focused ion beam (FIB) set-up (FEI; Helios 600). The fabricated tip is then analyzed (nanotube diameter and length) using a high-resolution scanning electron microscope (Zeiss; Ultra 55).

AFM Measurements. AFM measurements were made using an NTEGRA system and Smena head (NT-MDT). For the water pullout experiments, a special add-on, water reservoir, was used under ambient conditions (~23 °C). In the experiments, a nanotube affixed to a precalibrated AFM cantilever was used. The AFM was directed downward to land on the water surface until a cantilever deflection threshold was detected (which indicates that the water surface is being pierced by the nanotube tip). Immediately upon reaching the contact point, the nanotube was pulled out to fully remove the INT from the water by retraction of the z-piezo. The force acting on the nanotube during immersion and retraction was monitored through the cantilever deflection signal. During retraction, the cantilever was bent toward the water surface until it reached a peak attractive force (maximum bending of the cantilever), at which point the nanotube snapped away from the water. This critical force was equated with the pullout force. The water pullouts were repeated 10–20 times for each kind of nanotube experiment.

ESEM Pullout Experiments. The ESEM water pullouts were performed using an FEI XL-30 ESEM. The ESEM was equipped with a water-cooled thermoelectric stage (temperature controlled). A water film was created by condensation of water on a cooled (4.5–5 °C) stainless-steel stub and using a water vapor pressure ranging between 6.5 and 7 torr. A tip consisting of precalibrated AFM cantilever with a nanotube attached to it was then mounted on a nanomanipulator (Kliendiek; model MM3A-EM) inside an ESEM. This setup enabled a precise control of the tip movement with a precision of less than 10 nm. The tip was approached using a nanomanipulator (Fig. S1). The end of the nanotube was carefully brought into contact with the water film. Subsequently, the INT was slowly retracted, which led to development of a water meniscus. The meniscus gradually increased in size until the retraction distance where the nanotube tip separated from the water. The pullout force was calculated by Hooke's law, using the difference between the water protrusion maximal height and the tip height at the final location of the NT apex.

MD Simulations. MD simulations of all nanosystems have been performed using in-house code as for NVT ensembles ($T = 300$ K). Temperature was controlled in all simulations with the velocity scaling. Newton's equations of motion were

integrated with the time step of 2 fs via the Verlet leapfrog algorithm for 250,000 steps. The water film was initially annealed and equilibrated under the same conditions for 500,000 steps. The apex of the nanotube tip was initially positioned ~3 Å from the equilibrated water surface, which corresponded to the distance 25 Å from the substrate. Two velocities of the tip withdrawal have been tested for selected nanosystems as 0.025 and 0.25 Å/ps (2.5 and 25 m/s). No essential difference was established between these cases. Thus, the results presented in this work are given for the speed 0.25 Å/ps, which allowed testing of a more diverse set of nanotubes for the same computational time consumption.

The force-field level of theory was applied for these nanosecond simulations. Interactions within the H_2O film were treated in the framework of a flexible simple point charge (SPC) model in the parameterization (34). A WS_2 tip was considered as a body generating electrostatic and van der Waals fields in the framework of a universal force field (UFF) (35). The coupling between parameterization sets for H_2O and WS_2 parts was fulfilled using Coulomb and Lennard–Jones 12-6 potentials, where the missing heteronuclear parameters of 12-6 potentials were obtained after Lorentz–Berthelot mixing rules. Truncation at 12 Å for all short-range nonbonded interactions was applied. The long-range electrostatics interactions were computed without any restriction and approximation.

For the CCl_4, similar methodology was used, with some differences noted here: the molecule was modeled as a "spherical neutral superatom," where the intermolecular interaction between structureless CCl_4 molecules is modeled using a Lennard–Jones 12-6 potential (36). Truncation was at 20 Å. To account for the larger molecular size, larger nanotubes were used here [single-walled (21,21) and (28,28) or double-walled (21,21)@(28,28)]. Full description of all model setups can be found in the *Supporting Information*.

ACKNOWLEDGMENTS. We thank Bojana Visic for help in preparing the final figures. The ESEM and FIB imaging and fabrication were conducted at the Irving and Cherna Moskowitz Center for Nano and BioNano Imaging (Weizmann Institute). This work was supported by the Israel National Nano-Initiative, the Israel Science Foundation, and the H. Perlman Foundation. P.G. and A.E. acknowledge the support by Act 211 Government of the Russian Federation (Contract 02.A03.21.0006).

1. De Gennes P-G, Brochard-Wyart F, Quéré D (2013) *Capillarity and Wetting Phenomena: Drops, Bubbles, Pearls, Waves* (Springer Science and Business Media, New York).
2. Israelachvili J (2011) *Intermolecular and Surface Forces* (Academic, San Diego), Rev 3rd Ed.
3. Yong X, Zhang LT (2009) Nanoscale wetting on groove-patterned surfaces. *Langmuir* 25(9):5045–5053.
4. Bocquet L, Charlaix E (2010) Nanofluidics, from bulk to interfaces. *Chem Soc Rev* 39(3): 1073–1095.
5. Isa L, Lucas F, Wepf R, Reimhult E (2011) Measuring single-nanoparticle wetting properties by freeze-fracture shadow-casting cryo-scanning electron microscopy. *Nat Commun* 2:438.
6. Barber AH, Cohen SR, Wagner HD (2004) Static and dynamic wetting measurements of single carbon nanotubes. *Phys Rev Lett* 92(18):186103.
7. Boncel S, Walczak KZ, Koziol KKK (2011) Dynamics of capillary infiltration of liquids into a highly aligned multi-walled carbon nanotube film. *Beilstein J Nanotechnol* 2: 311–317.
8. Yum K, Yu M-F (2006) Measurement of wetting properties of individual boron nitride nanotubes with the Wilhelmy method using a nanotube-based force sensor. *Nano Lett* 6(2):329–333.
9. Tran MQ, Cabral JT, Shaffer MS, Bismarck A (2008) Direct measurement of the wetting behavior of individual carbon nanotubes by polymer melts: The key to carbon nanotube-polymer composites. *Nano Lett* 8(9):2744–2750.
10. Dujardin E, Ebbesen TW, Hiura H, Tanigaki K (1994) Capillarity and wetting of carbon nanotubes. *Science* 265(5180):1850–1852.
11. Kakade BA, Pillai VK (2008) Tuning the wetting properties of multiwalled carbon nanotubes by surface functionalization. *J Phys Chem C* 112(9):3183–3186.
12. Rossi MP, et al. (2004) Environmental scanning electron microscopy study of water in carbon nanopipes. *Nano Lett* 4(5):989–993.
13. Supple S, Quirke N (2004) Molecular dynamics of transient oil flows in nanopores I: Imbibition speeds for single wall carbon nanotubes. *J Chem Phys* 121(17):8571–8579.
14. Ugarte D, Chatelain A, De Heer WA (1996) Nanocapillarity and chemistry in carbon nanotubes. *Science* 274(5294):1897–1899.
15. Barber AH, Cohen SR, Wagner HD (2005) External and internal wetting of carbon nanotubes with organic liquids. *Phys Rev B* 71(11):115443.
16. Tsang SC, Chen YK, Harris PJF, Green MLH (1994) A simple chemical, method of opening and filling carbon nanotubes. *Nature* 372(6502):159–162.
17. Tenne R, Margulis L, Genut M, Hodes G (1992) Polyhedral and cylindrical structures of tungsten disulphide. *Nature* 360(6403):444–446.
18. Lalwani G, et al. (2013) Tungsten disulfide nanotubes reinforced biodegradable polymers for bone tissue engineering. *Acta Biomater* 9(9):8365–8373.
19. Naffakh M, Remškar M, Marco C, Gómez-Fatou MA, Jiménez I (2011) Towards a new generation of polymer nanocomposites based on inorganic nanotubes. *J Mater Chem* 21(11):3574–3578.
20. Díez-Pascual AM, Naffakh M, Marco C, Ellis G (2012) Rheological and tribological properties of carbon nanotube/thermoplastic nanocomposites incorporating inorganic fullerene-like WS_2 nanoparticles. *J Phys Chem B* 116(27):7959–7969.
21. Ataca C, Ciraci S (2012) Dissociation of H_2O at the vacancies of single-layer MoS 2. *Phys Rev B* 85(19):195410.
22. Chow PK, et al. (2015) Wetting of mono and few-layered WS_2 and MoS_2 films supported on Si/SiO_2 substrates. *ACS Nano* 9(3):3023–3031.
23. Ghuman KK, Yadav S, Singh CV (2015) Adsorption and dissociation of H_2O on monolayered MoS_2 edges: Energetics and mechanism from ab initio simulations. *J Phys Chem C* 119(12):6518–6529.
24. Adamson AW (1990) *Physical Chemistry of Surfaces* (Wiley, New York), 5th Ed.
25. Kaplan-Ashiri I, et al. (2006) On the mechanical behavior of WS_2 nanotubes under axial tension and compression. *Proc Natl Acad Sci USA* 103(3):523–528.
26. Washburn EW (1921) The dynamics of capillary flow. *Phys Rev* 17(3):273–283.
27. Joswiak MN, Duff N, Doherty MF, Peters B (2013) Size-dependent surface free energy and Tolman-corrected droplet nucleation of TIP4P/2005 water. *J Phys Chem Lett* 4(24): 4267–4272.
28. Caupin F, Cole MW, Balibar S, Treiner J (2008) Absolute limit for the capillary rise of a fluid. *Europhys Lett* 82(5):56004.
29. Boruvka L, Neumann A (1977) Generalization of the classical theory of capillarity. *J Chem Phys* 66(12):5464–5476.
30. Luan B, Zhou R (2016) Wettability and friction of water on a MoS_2 nanosheet. *Appl Phys Lett* 108(13):131601.
31. Levi R, Bitton O, Leitus G, Tenne R, Joselevich E (2013) Field-effect transistors based on WS_2 nanotubes with high current-carrying capacity. *Nano Lett* 13(8):3736–3741.
32. Margolin A, Rosentsveig R, Albu-Yaron A, Popovitz-Biro R, Tenne R (2004) Study of the growth mechanism of WS_2 nanotubes produced by a fluidized bed reactor. *J Mater Chem* 14(4):617–624.
33. Zak A, Sallacan-Ecker L, Margolin A, Genut M, Tenne R (2009) Insight into the growth mechanism of WS_2 nanotubes in the scaled-up fluidized-bed reactor. *Nano* 4(02): 91–98.
34. Mark P, Nilsson L (2001) Structure and dynamics of the TIP3P, SPC, and SPC/E water models at 298 K. *J Phys Chem A* 105(43):9954–9960.
35. Rappé AK, Casewit CJ, Colwell K, Goddard Iii W, Skiff W (1992) UFF, a full periodic table force field for molecular mechanics and molecular dynamics simulations. *J Am Chem Soc* 114(25):10024–10035.
36. Marzec M, Kuchta B, Firlej L (2007) Adsorption and phase transitions in adsorbed systems: Structural properties of CCl_4 layers adsorbed on a graphite surface. *J Mol Model* 13(4):537–542.
37. Kralj-Iglič V, Remškar M, Vidmar G, Fošnarič M, Iglič A (2002) Deviatoric elasticity as a possible physical mechanism explaining collapse of inorganic micro and nanotubes. *Phys Lett A* 296(2):151–155.
38. Ordejón P, Artacho E, Soler JM (1996) Self-consistent order-N density-functional calculations for very large systems. *Phys Rev B Condens Matter* 53(16):R10441–R10444.
39. Soler JM, et al. (2002) The SIESTA method for ab initio order-N materials simulation. *J Phys Condens Matter* 14(11):2745.
40. Hohenberg P, Kohn W (1964) Inhomogeneous electron gas. *Phys Rev* 136:B864.
41. Kohn W, Sham LJ (1965) Self-consistent equations including exchange and correlation effects. *Phys Rev* 140:A1133.
42. Perdew JP, Burke K, Ernzerhof M (1996) Generalized gradient approximation made simple. *Phys Rev Lett* 77(18):3865–3868.
43. Troullier N, Martins JL (1991) Efficient pseudopotentials for plane-wave calculations. *Phys Rev B Condens Matter* 43(3):1993–2006.
44. Moreno J, Soler JM (1992) Optimal meshes for integrals in real- and reciprocal-space unit cells. *Phys Rev B Condens Matter* 45(24):13891–13898.
45. Fernández-Serra MV, Artacho E (2004) Network equilibration and first-principles liquid water. *J Chem Phys* 121(22):11136–11144.
46. Jorgensen WL, et al. (1983) Comparison of simple potential functions for simulating liquid water. *J Chem Phys* 79(2):926–935.